2009 American Control Conference
Hyatt Regency Riverfront, St. Louis, MO, USA
June 10-12, 2009

Modeling the Effect of Fuel Ethanol Concentration on Cylinder Pressure Evolution in Direct-Injection Flex-Fuel Engines

Nestor H. Oliverio, Li Jiang, Hakan Yilmaz and Anna G. Stefanopoulou

Abstract— **A physics-based lumped-parameter model for the cylinder pressure evolution during the compression stroke in Flex-Fuel Direct-Injection (DI) engines is developed in this paper. The proposed model captures the fuel vaporization process for ethanol-gasoline fuel blends and the associated charge cooling effect. In addition, a detection residue is introduced to process cylinder pressure measurements under two different fuel injection patterns and extract the charge cooling effect caused by fuel vaporization during the compression stroke. The residues calculated from the proposed model were validated with those generated from experimental cylinder pressure for different gasoline-ethanol blends and various speeds and loads on a 2.0 L Turbocharged Spark Ignited Direct Injection (SIDI) engine with Variable Valve timing (VVT). Residues generated from both measured and modeled cylinder pressure exhibit a monotonic correlation with the fuel ethanol content for all the tested engine operating conditions. The promising results point to the potential of the proposed model to be integrated with the residue generation algorithm into a real-time model-based scheme for ethanol detection.**

I. Introduction

Ethanol is a renewable fuel with a, potentially, neutral CO_2 cycle and recognized as a promising substitute for conventional gasoline. In fact, current fuel standards (e.g. ASTM D4814) have already allowed up to 10% ethanol content for regular gasoline and the use of E85 (85% ethanol and 15% gasoline in volume). Today's Flexible-fuel vehicles (FFV) have been equipped with the capability of running on any ethanol-gasoline blend from E0 to E85. However, dedicated engine control schemes are yet to be developed to exploit some of the advantageous fuel properties of ethanol and thus improve fuel economy and engine performance. For instance, since ethanol has a higher octane number, the ignition timing could be adjusted accordingly to take advantage of its higher knock resistance and thus maximize the engine output power. Table I compares the most relevant ethanol and gasoline properties. Such engine control optimization or more basic adaptations, such as cold-start fuel injection amount, require the knowledge or estimation of the ethanol concentration in the fuel.

Ethanol sensors [1][2] have been developed to detect the fuel ethanol concentration by placing them in the tank or in the fuel line. However, they are not widely used in production vehicles mainly due to the high additional cost. The ethanol content in the fuel can also be indirectly detected by means of the closed-loop air/fuel ratio correction signal based on the Exhaust Gas Oxygen (EGO) sensor [3][4]. Although ethanol detection via the EGO sensor can achieve an acceptable accuracy, the detection speed is slow and it can not be used at engine startup [5] due to the unavailability of the EGO sensor. Furthermore, this method might misinterpret other faults, such as mass air flow sensor or injector drifts, for a change in ethanol concentration [6] [7]. Various methods have also been developed to determine the fuel composition via cylinder pressure sensors by exploiting the effects of ethanol concentration on the combustion behavior [8][9] . However, to some extent, these approaches overlap with the EGO-based method because, they all rely on combustion-related fuel properties.

TABLE I
Ethanol and Gasoline properties

	Gasoline	Ethanol
RON	92	111
Stoichiometric A/F ratio	14.3	9.0
Density (g/cm^3)	0.74	0.79
Boiling Point(°C)	20-300	78.5
Heat of Combustion (MJ/kg)	42.4	26.8
Enthalpy of vaporization(kJ/kg)	420	845

Due to the different enthalpy of vaporization between gasoline and ethanol, fuels with different ethanol content introduce different cooling effects on the cylinder charge. The additional charge cooling effect caused by ethanol injection is employed in [10] to improve engine efficiency and performance. The present work studies the charge cooling effect for different fuel ethanol contents, its impact on the cylinder pressure evolution and the feasibility of its use for fuel ethanol content estimation.

First, a physical lumped-parameter model with emphasis on fuel vaporization and the associated charge cooling effect is described in Section III. Then, the effects of fuel ethanol content on the cylinder pressure are discussed in Section IV under the view of the presented model. In addition, the concept of a detection residue is introduced to extract the charge cooling from cylinder pressure measurements during the compression stroke by exploiting the effects of two different injection patterns. Finally, the model calibration procedure is described in Section V, and experimental results obtained on a 2.0 L Turbocharged SIDI VVT engine at various speeds and loads for different ethanol-gasoline fuel blends are discussed. The results validate the proposed model and show a monotonic correlation between the extracted residues and the fuel ethanol content.

This work is funded by the U.S. Department of Energy and Robert Bosch LLC.

N.H. Oliverio (neoliver@umich.edu) and A.G. Stefanopoulou (annastef@umich.edu) are with Electrical and Mechanical Engineering departments, respectively, at the University of Michigan, Ann Arbor. L. Jiang (li.jiang@us.bosch.com) and H. Yilmaz (hakan.yilmaz@us.bosch.com) are with Robert Bosch LLC, Farmington Hills.

978-1-4244-4524-0/09/$25.00 ©2009 AACC

II. Nomenclature

In the rest of this paper, the variables to be used are: V for volume, T for temperature, P for pressure, Q for heat, m for mass, y for mass fraction or vapor concentration, Y for molar fraction, VP for vapor pressure, PP for partial pressure, and M for molecular weight.

The subscripts to be used are: a for air, eg for exhaust gases, g for the mixture of air and exhaust gases, cyl for total cylinder gaseous charge including fuel vapor, $fl[\mu]$ for liquid fuel spray $[\mu]$, $fv[\mu]$ for vaporized fuel from spray $[\mu]$, $fl[\mu], inj$ for liquid fuel injected during injection period $[\mu]$. $\mu \in \{i_s, c_s\}$ indicates the fuel injected during the intake stroke, $[i_s]$, or the compression stroke, $[c_s]$. When the subscript $[\mu]$ is skipped, the associated variable refers to the total amount over both injections. The superscripts are used to indicate a particular fuel component.

III. Physics-Based Model

In order to further investigate the effects of fuel ethanol content on the cylinder pressure evolution presented in [11], a lumped-parameter model is developed with emphasis on the fuel vaporization process, and its associated charge cooling effect during the compression stroke. Such a model needs to capture the overall intake stroke behavior, i.e. charge characteristic at Intake Valve Closure (IVC), and reproduce the crank-resolved evolution of the cylinder pressure during the compression stroke for different engine operating points (speed and intake mass air flow), fuel ethanol contents, and injection conditions (pattern, timing, duration, pressure).

During intake and compression strokes, two different matter states coexist inside the cylinder:

1) gaseous cylinder charge form by fresh air, exhaust gases and vaporized fuel, and
2) liquid fuel spray.

Different injection periods result in independent liquid fuel spray systems. In particular in this work, two injection periods are used for ethanol detection purposes as explained in Section IV. The first injection, $[i_s]$, occurs early in the intake phase while, the second one, $[c_s]$, takes place early in the compression stroke. The interaction among the three resulting thermodynamic systems is depicted in Fig. 1. Basically, the liquid fuel sprays absorb heat from the gaseous cylinder charge while adding the vaporized fuel into it.

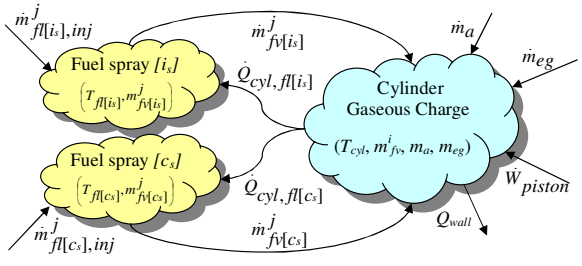

Fig. 1. Thermodynamical systems inside the cylinder

The intake-compression process modeling can be divided in five closely interrelated sub-models:

A) multi-component fuel model,
B) gaseous cylinder charge model,
C) liquid fuel sprays ($[i_s]$ and $[c_s]$) model,
D) fuel droplet vaporization model, and
E) cylinder charge estimation at IVC.

A. Multi-Component Fuel Model

A multi-component model is used to capture the behavior of gasoline-ethanol fuel blends inside the cylinder [12]. The mass fraction of each component in the injected fuel is given by:

$$y^j_{fl,inj} = y^j_{fl,gsl}(1-e) + y^j_{fl,etoh}e, \tag{1}$$

where $e \in [0,1]$ denotes the mass fraction of ethanol in the ethanol-gasoline blend. The composition for gasoline and pure ethanol are given in Table II [12].

TABLE II
Components mass fraction for gasoline and pure ethanol

#	Component Name	Gasoline $y^j_{fl,gsl}$	Ethanol $y^j_{fl,etoh}$
1	Ethanol	0	1
2	Isopentane	0.16	0
3	Toluene	0.255	0
4	n-Butane	0.04	0
5	n-Hexane	0.025	0
6	n-Tridecane	0.02	0
7	n-Octane	0	0
8	123TM-Benzene	0.18	0
9	224TM-Pentane	0.32	0

B. Gaseous Cylinder Charge Model

The gaseous cylinder charge is composed by a mixture of fresh air, exhaust gases and vaporized fuel. The crank-resolved evolution of the mixture temperature, pressure and composition, during the compression stroke are derived applying conservation of energy and mass [13][14]. The state equations for the gaseous charge during compression stroke, between IVC and spark ignition, i.e. $t \in (t_{ivc}, t_{ign})$, are:

$$\begin{aligned}\frac{dT_{cyl}}{dt} = &-\frac{(n_c-1)\cdot T_{cyl}}{V_{cyl}}\dot{V}_{cyl} - \frac{\beta\cdot(T_{cyl}-T_{wall})\,V_{cyl}}{c_{v,cyl}} \\ &- \sum_{\mu=\{i_s,c_s\}} \frac{\dot{Q}_{cyl,fl[\mu]}}{c_{v,cyl}m_{cyl}} - \sum_{j=1}^{N}\frac{u^j_{fv}(T_{cyl}) - u_g(T_{cyl})}{c_{v,cyl}m_{cyl}}\dot{f}^j \\ &+ \sum_{\mu=\{i_s,c_s\}}\sum_{j=1}^{N}\frac{h^j_{fv[\mu]}(T_{fl[\mu]}) - u_{cyl}}{c_{v,cyl}m_{cyl}}\dot{m}^j_{fv[\mu]}\end{aligned} \tag{2}$$

$$\frac{dm^j_{fv}}{dt} = \sum_{\mu=\{i_s,c_s\}}\dot{m}^j_{fv[\mu]}, \qquad \text{for } j = 1,\ldots,N=9, \tag{3}$$

$$\frac{dm_a}{dt} = 0, \qquad \frac{dm_{eg}}{dt} = 0, \tag{4}$$

where, $c_{v,cyl}$ is the equivalent cylinder charge heat capacity, u_g, u^j_{fv}, and u_{cyl} are the internal energies of the cylinder gases, each fuel vapor component, and total cylinder charge, respectively, and $h^j_{fv[\mu]}$ is the enthalpy of each fuel vapor component. The first term in the right hand side of Eq. (2) characterizes the polytropic compression process while

the rest are deviations due to mass and heat exchange. The parameter n_c is the polytropic compression coefficient and β is the heat transfer coefficient between gaseous mixture and cylinder walls. The average chamber walls temperature, T_{wall}, the cylinder volume, V_{cyl}, and its derivative, $\dot{V}_{cyl}$, are inputs generated from measurements. The heat flow from the cylinder charge to the liquid fuel sprays, $\dot{Q}_{cyl,fl[\mu]}$, the sprays rate of vaporization, $\dot{m}^j_{fv[\mu]}$, and the sprays temperatures, $T_{fl[\mu]}$, are determined by the *Liquid Fuel Spray Model* in Eq. (17), (14), and (13), respectively. The states initial conditions at IVC, $T_{cyl,0}$, $m^j_{fv,0}$, $m_{a,0}$, and $m_{eg,0}$ are generated by the *Cylinder Charge Estimation at IVC*.

The cylinder pressure is then derived using the ideal gas law,

$$P_{cyl} = \frac{m_{cyl} R T_{cyl}}{V_{cyl}}. \tag{5}$$

The total mass inside the cylinder, m_{cyl}, is:

$$m_{cyl} = m_g + m_{fv}\ , \qquad m_g = m_a + m_{eg}, \tag{6}$$

where, m_g is the total mass of gases in the cylinder charge, m_a is the mass of air, and m_{eg} is the mass of exhaust gases. The total fuel vapor mass, m_{fv}, and its derivative, $\dot{m}_{fv}$, are:

$$m_{fv} = \sum_{j=1}^{N} m^j_{fv}\ , \qquad \dot{m}_{fv} = \sum_{j=1}^{N} \dot{m}^j_{fv}. \tag{7}$$

The fuel fraction, f, the fuel fraction of each component, f^j, and its derivative, $\dot{f}^j$, are:

$$f^j = \frac{m^j_{fv}}{m_{cyl}}\ ,\ f = \sum_{j=1}^{N} f^j\ ,\ \dot{f}^j = \frac{\dot{m}^j_{fv}}{m_{cyl}} - \frac{m^j_{fv}\dot{m}_{fv}}{m^2_{cyl}}. \tag{8}$$

C. Liquid Fuel Spray Model

The fuel injected into the cylinder forms a cloud of liquid droplets which vaporizes while absorbing heat from the cylinder charge. Fuel clouds generated by different injection periods are modeled as different thermodynamic systems which do not interact directly with each other. The subscript $[\mu]$ denotes indistinctly any fuel spray. The assumptions used to model each fuel spray are:

1) The droplets do not interact with each other, only with the gaseous cylinder charge.
2) All the droplets in a spray are spherical, symmetrical, and identical to each other.
3) The liquid fuel density, $\rho_{d[\mu]}$, and temperature, $T_{fl[\mu]}$, are homogeneous along the entire droplet, that is, the liquid fuel diffusion coefficient and heat conductivity are infinite.
4) There is no wall wetting, i.e., no droplet leaves the spray to form a puddle.
5) The fuel rail pressure, P_{inj}, and the cylinder pressure, P_{cyl}, are constant during the fuel injection period.

The liquid fuel spray is characterized by the number of droplets suspended in the cylinder charge, $N_d[\mu]$, the diameter and surface area of the droplets, $d_d[\mu]$ and $A_d[\mu]$, and the droplet density, $\rho_{d[\mu]}$:

$$N_{d[\mu]}(t) = \frac{m_{fl[\mu]}(t-\tau_d) + m_{fv[\mu]}(t-\tau_d)}{\frac{\pi}{6}\left(d_{d,0}\right)^3 \cdot \rho_{fl,inj}}, \tag{9}$$

$$d_{d[\mu]} = \left(\frac{6 \cdot \sum_{j=1}^{N} m^j_{fl[\mu]}}{\pi \cdot N_{d[\mu]} \cdot \rho_{d[\mu]}}\right)^{1/3}, \tag{10}$$

$$A_{d[\mu]} = \pi \cdot d^2_{d[\mu]}, \tag{11}$$

$$\rho_{d[\mu]} = \frac{\sum_{j=1}^{N} m^j_{fl[\mu]}}{\sum_{l=1}^{N} m^l_{fl[\mu]} / \rho^j_{fl[\mu]}}, \tag{12}$$

where, $\rho_{fl[\mu],inj}$ is the density of the injected fuel; and τ_d and $d_{d[\mu],0}$ are parameters to specify the spray formation delay, and the initial droplet diameter, respectively.

The dynamic states for the liquid fuel spray are the spray fuel temperature, $T_{fl[\mu]}$, and the total mass of each liquid fuel component in the spray, $m^j_{fl[\mu]}$. The state equations are derived through conservation of mass and energy as follows:

$$\frac{dT_{fl[\mu]}}{dt} = \sum_{j=1}^{N} \frac{c^j_{p,fl[\mu]} T_{fl[\mu],inj} - c^j_{v,fl[\mu]} T_{fl[\mu]}}{m_{fl[\mu]} c_{v,fl[\mu]}} \dot{m}^j_{fl[\mu],inj} + \frac{\dot{Q}_{cyl,fl[\mu]}}{m_{fl[\mu]} c_{v,fl[\mu]}} - \frac{\sum_{j=1}^{N} Q^j_{vap[\mu]} \dot{m}^j_{fv[\mu]}}{m_{fl[\mu]} c_{v,fl[\mu]}} \tag{13}$$

$$\frac{dm^j_{fl[\mu]}}{dt} = \dot{m}^j_{fl[\mu],inj} - \dot{m}^j_{fv[\mu]}, \quad \text{for } j = 1, \ldots, N, \tag{14}$$

where, the injected flow of each fuel component, $\dot{m}^j_{fl[\mu],inj}$, is given by Eq. (15), and the total injected flow, $\dot{m}_{fl[\mu],inj}$ and its temperature, $T_{fl[\mu],inj}$, are measured inputs.

$$\dot{m}^j_{fl[\mu],inj} = y^j_{fl,inj} \cdot \dot{m}_{fl[\mu],inj}, \quad \text{for } j = 1, \ldots, N. \tag{15}$$

The vaporization rate for each fuel component in the spray, $\dot{m}^j_{fv[\mu]}$, and the liquid fuel spray mass, $m_{fl[x]}$, are:

$$\dot{m}^j_{fv[\mu]} = N_{d[\mu]} \cdot \dot{m}^j_{d[\mu]}, \quad m_{fl[x]} = \sum_{j=1}^{N} m^j_{fl[\mu]}, \tag{16}$$

where, $\dot{m}^j_{d[\mu]}$ is the droplet rate of vaporization determined by the *Fuel Droplet Vaporization Model* in Eq. (18).

The heat flow from the cylinder charge to the spray is:

$$\dot{Q}_{cyl,fl[\mu]} = \alpha(1 + \kappa \dot{V}_{cyl})\sqrt{P_{cyl}} N_{d[\mu]} A_{d[\mu]} \cdot (T_{cyl} - T_{fl[\mu]}) + \gamma \sum_{j=1}^{N} Q^j_{vap[\mu]} \cdot \dot{m}^j_{fv[\mu]}, \tag{17}$$

where, the parameter α is the heat transfer coefficient between the droplets and the cylinder charge, κ captures the influence of the charge turbulence on the heat transfer process, and γ is a heat flow balance coefficient which allows to capture the important effect of the actual *finite* fuel heat conductivity with a lumped-parameter model (assumptions 2 and 3). Due to *finite* heat conductivity, the fuel vaporization causes a superficial droplet temperature drop which results in a heat flow to the droplet surface from both,

the surrounding cylinder charge and the inner-droplet fuel. The heat flow balance coefficient, γ, establishes the overall amount of heat absorbed from the cylinder charge and the inner-droplet, respectively. In the current model calibration, $\gamma = 0.8$ was adopted to reproduce the measured instantaneous charge cooling effect and the fuel vaporization characteristics presented in [15].

D. Fuel Droplet Vaporization Model

The vaporization rate for each fuel component in the droplet is modeled using the gas diffusion law and following the same concepts first introduced in [16] and later modified in [17][12] to model fuel puddle dynamics and in [18][19] to model fuel droplet vaporization. The rate of vaporization of each fuel component in the droplet is:

$$\dot{m}^j_{d[\mu]} = \frac{y^j_{fv,s[\mu]}(B_{[\mu]}+1) - y^j_{fv,\infty}}{B_{[\mu]}}\dot{m}_{d[\mu]}, \tag{18}$$

where, $y^j_{fv,s[\mu]}$ and $y^j_{fv,\infty}$ are the vapor concentration of each fuel component at the droplet surface and infinite distance, respectively. The Spalding number, $B_{[\mu]}$, and the total droplet vaporization rate, $\dot{m}_{d[\mu]}$, are:

$$B_{[\mu]} = \frac{y_{fv,s[\mu]} - y_{fv,\infty}}{1 - y_{fv,s[\mu]}}, \tag{19}$$

$$\dot{m}_{d[\mu]} = k_{evap} \cdot \rho_{d[\mu]} \cdot d_{d[\mu]} \cdot D_{[\mu]} \cdot \ln(B_{[\mu]}+1), \tag{20}$$

where, $\rho_{d[\mu]}$ and $d_{d[\mu]}$ are the spray average droplet density and diameter, respectively. $D_{[\mu]}$ is the fuel vapor diffusion coefficient and k_{evap} is the vaporization constant which is empirically determined. The total vapor concentration at the droplet surface, $y_{fv,s[\mu]}$, and infinite distance, $y_{fv,\infty}$, are:

$$y_{fv,s[\mu]} = \sum_{j=1}^{N} y^j_{fv,s[\mu]}, \qquad y_{fv,\infty} = \sum_{j=1}^{N} y^j_{fv,\infty}. \tag{21}$$

The vapor concentration at the droplet surface for each fuel component is based on Raoult's law:

$$y^j_{fv,s[\mu]} = \frac{Y^j_{fl[\mu]}\mathrm{VP}^j_{fl}M^j_{fv}}{PP_{g,s[\mu]}M_g + \sum_{j=1}^{N} Y^j_{fl[\mu]}\mathrm{VP}^j_{fl}M^j_{fv}}, \tag{22}$$

where, $\mathrm{VP}^j_{fl} = \mathrm{VP}^j_{fl}\left(T_{fl[\mu]}\right)$ is the vapor pressure of each fuel component at temperature $T_{fl[\mu]}$, $Y^j_{fl[\mu]}$ is the molar concentration of each fuel component in the droplet, and $PP_{g,s}$ is the partial pressure of gas (fresh air and exhaust gases) at the droplet surface given by Eq. (23)

$$PP_{g,s[\mu]} = P_{cyl} - \sum_{j=1}^{N} Y^j_{fl[\mu]}\mathrm{VP}^j_{fl}(T_{fl[\mu]}). \tag{23}$$

The vapor concentration at infinite distance for each fuel component is computed using the partial vapor pressure of the corresponding fuel component in the gaseous mixture, PP^i_{fv}, and the partial pressure of gas in the cylinder, PP_g:

$$y^j_{fl,\infty} = \frac{\mathrm{PP}^j_{fv}M^j_{fv}}{\mathrm{PP}_g M_g + \sum_{j=1}^{N}\mathrm{PP}^j_{fv}M^j_{fv}}. \tag{24}$$

E. Cylinder Charge Estimation at IVC

The estimation of the initial conditions of the model states at IVC, $T_{cyl,0}$, $m_{cyl,0}$, $m_{eg,0}$, $m^j_{fv,0}$, $m^j_{fl[i_s],0}$, and $T_{fl[i_s],0}$, is based on energy balance at IVC and the ideal gas law [20]:

$$\begin{aligned}&\left(c_{v,a}m_{a,0} + c_{v,eg}m_{eg,0} + \sum_{j=1}^{N} c^j_{v,fv}m^j_{fv,0}\right)\cdot T_{cyl,0}\\ &= c_{p,a}m_{a,0}T_a + c_{p,eg}m_{eg,0}\hat{T}_{eg} + H_{fv,0} - P_{cyl,0}V_{cyl,0}\\ &- Q_{fl,0} + \beta_{int}\tau_{int}m_{cyl,0}\left(T_{wall} - T_{cyl,0}\right),\end{aligned} \tag{25}$$

$$T_{cyl,0} = \frac{P_{cyl,0}V_{cyl,0}}{m_{cyl,0}R}, \tag{26}$$

where, τ_{int} is the intake period duration, and the parameter β_{int} is the heat transfer coefficient between the cylinder gaseous charge and chamber walls during the intake period.

The amount of air inducted during intake, $m_{a,0}$, the intake air temperature, T_a, the mass of fuel injected during intake, $m_{fl[i_s],inj}$, the cylinder pressure at IVC, $P_{cyl,0}$, and the average cylinder wall temperature, T_{wall}, are determined from measurements. The amount of fuel vaporized by IVC, $m^j_{fv,0}$, the heat transfer from the cylinder charge to the fuel spray, $Q_{fl,0}$, and the enthalpy of the vaporized fuel, $H_{fv,0}$, are calculated as:

$$m^j_{fv,0} = \int_{t_{eoj[i_s]}}^{ivc} \dot{m}^j_{fv}(t)\cdot dt \tag{27}$$

$$Q_{fl,0} = \int_{t_{eoj[i_s]}}^{ivc} \dot{Q}_{cyl,fl[i_s]}(t)\cdot dt \tag{28}$$

$$H_{fv,0} = \int_{t_{eoj[i_s]}}^{ivc} \left(\sum_{j=1}^{N} c^j_{p,fv}\dot{m}^j_{fv[i_s]}(t)T_{fl[i_s]}(t)\right)\cdot dt, \tag{29}$$

where, $t_{eoj[i_s]} < ivc$ is the end of the intake-stroke injection; and $\dot{m}^j_{fv[i_s]}(t)$, $\dot{Q}_{fl[i_s],0}(t)$, and $T_{fl[i_s]}(t)$ are given in Eq. (16), (17), and (13), respectively, and computed running the *Fuel Droplet Vaporization Model* and the *Liquid Fuel Spray Model* under the following assumptions:

$$T_{cyl}(t) = T_{cyl,0};\ P_{cyl}(t) = P_{cyl,0}$$
$$V_{cyl}(t) = V_{ivc};\ m_a(t) = m_{a,0};\ m_{eg}(t) = m_{eg,0}$$

Finally, $T_{cyl,0}$, $m_{eg,0}$, $m^j_{fv,0}$, $m^j_{fl[i_s],0}$, and $T_{fl[i_s],0}$ are determined by solving iteratively Eq. (25) through (29).

In addition, due to the high variance in the exhaust gas temperature measurement, an estimation, $\hat{T}_{eg}$, needs to be used instead. $\hat{T}_{eg}$ is generated by an iterative estimator which utilizes the compression and expansion pressure traces to generate a more accurate value for the exhaust temperature.

IV. Effect of Ethanol Concentration

As shown in Table I, the vaporization enthalpy of ethanol is much higher than that of gasoline. As a result, a stronger charge cooling effect is expected for fuel blends with higher ethanol content. When fuel is injected during the intake stroke, the charge cooling effect improves the engine volumetric efficiency by allowing more air into the cylinders [18], but has little or no effect on the cylinder pressure. Therefore,

an additional injection is introduced during the compression stroke, when all valves are closed, to enable the detection of such effect on the cylinder pressure. Fig. 2 shows simulation results for E0 and E85 under the following two injection modes:

1) **Single injection (Si) mode:** all the fuel is injected during the intake stroke.
2) **Split injection (Sp) mode:** a fraction of the fuel is injected during the intake stroke, and the rest is injected early during compression stroke after IVC.

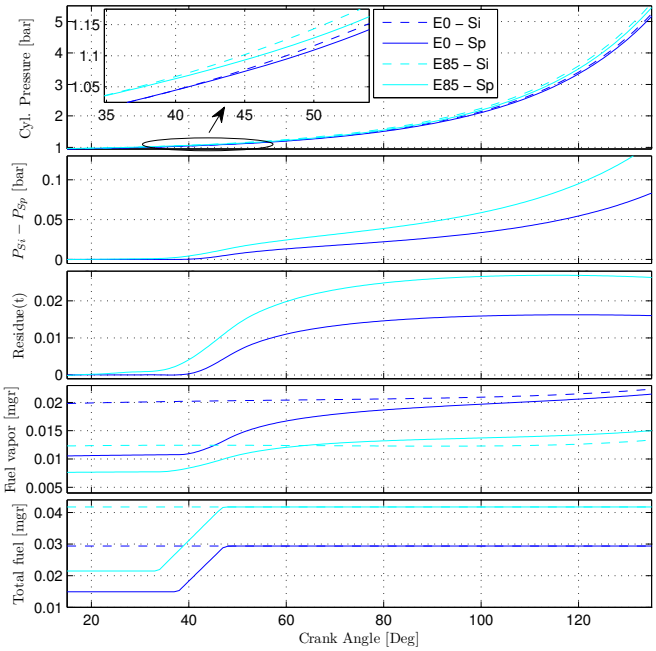

Fig. 2. Simulated results at engine speed of 2500RPM and intake airflow rate of 170kg/hr under Single (Si) and Split (Sp) injection modes for E0 and E85. a) Cylinder pressure. b) Pressure difference between Single and Split modes. c) Amount of vaporized fuel. d) Total amount of injected fuel.

It can be observed in Fig. 2.a that the cylinder pressures under the single injection mode are higher than those under the split mode for the same engine operating conditions. Fig. 2.b corroborates the initial hypothesis that fuels with higher ethanol content introduced stronger charge cooling effects, and thus results in a larger difference in the cylinder pressures under both injection modes. However, the differences observed in the cylinder pressure during the compression stroke due to fuel vaporization ranges from 1% to 5% of the pressure magnitude depending on the engine operating condition and fuel blend. Therefore, a detection residue is utilized to extract such small effect from cylinder pressure measurements, while eliminating or minimizing error sources such as: quantization and measurement noise, pressure sensor nonlinearities and pegging errors, and disturbances.

A. Detection Residue

As discussed above, fuel injection during the compression stroke introduces a drop in the cylinder pressure associated with the charge cooling effect caused by the fuel vaporization. Inspired this fact, the detection residue is computed by subtracting the cylinder pressures during the compression stroke under Single and Split injection modes, in order to accurately extract the charge cooling caused by the 2nd fuel injection. The residue generation introduced in [12] consists of a signal conditioning block and the actual residue computation algorithm as shown in Fig. 3.

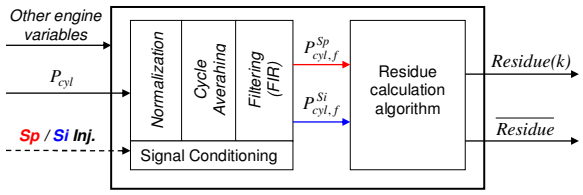

Fig. 3. High-level block diagram of the residue generation algorithm.

1) Signal conditioning: The signal conditioning consists of 3 stages: normalization, cycle-average and filtering. It is intended to minimize the following sources of error.

- Engine conditions variations.
- Cycle-to-cycle variations in the engine behavior.
- Pressure sensor measurement and quantization noise.
- Disturbances and unmodeled fast dynamics.

2) Residue Computation: The residue is calculated as:

$$Residue(k) = \log\left(P_0^{Si}(k)\right) - \log\left(P_0^{Sp}(k)\right), \qquad (30)$$

where P_0^{Si} and P_0^{Sp} are corrected cylinder pressures under Single and Split injection modes, respectively. A correction is needed because the methodology is very sensitive to offset errors which translate directly to the generated residue. Cylinder pressure sensors are very likely to have offset issues because they are composed of a piezoelectric material and output the derivative of the measured pressure. To construct the actual pressure measurement, the sensor output needs to be integrated, and periodically referenced following some pegging procedures. Various methods have been proposed in literature to address the non-trivial pegging problem [21][22][20][23]. Pegging errors also affect the simulation through the initial conditions; this issue will be discussed in detail in Section V. The following proposed correction ensures zero mean initial value for the residue:

$$P_0^{Si}(k) = P_{cyl,f}^{Si}(k) + \frac{\sum_{j=k_{SoCp}}^{k_{SoIj2}-\Delta} P_{cyl,f}^{Sp}(j) - P_{cyl,f}^{Si}(j)}{2\cdot\left(k_{SoIj2} - \Delta - k_{SoCp}\right)} \qquad (31)$$

$$P_0^{Sp}(k) = P_{cyl,f}^{Sp}(k) - \frac{\sum_{j=k_{SoCp}}^{k_{SoIj2}-\Delta} P_{cyl,f}^{Sp}(j) - P_{cyl,f}^{Si}(j)}{2\cdot\left(k_{SoIj2} - \Delta - k_{SoCp}\right)}, \qquad (32)$$

where $P_{cyl,f}^{Si}(k)$ and $P_{cyl,f}^{Sp}(k)$ are the conditioned cylinder pressure traces generated by the signal conditioning block for Single and Split injection modes, respectively. k_{SoIj2} and k_{SoCp} are the indexes corresponding to the start of the 2nd injection and the compression stroke, respectively, while Δ accounts for the spread of the charge cooling due to the filtering and vaporization dynamics.

In order to generate a single-value feature which facilitates the trend analysis and model validation, the mean-residue is introduced in Eq.(33).

$$\overline{Residue} = \frac{\sum_{j=k_{SoCp+100°}}^{k_{SoCp+140°}} Residue(j)}{k_{SoCp+140°} - k_{SoCp+100°}}, \quad (33)$$

where, the interval $[100°, 140°]$ corresponds to the steady part of $Residue(k)$ toward the end of compression.

B. Residue vs Fuel Ethanol Content

The simulated results in Fig. 2.c show the time-varying residues reach a higher steady final value for E85 than E0. This trend is corroborated by the experimental results presented in section V, where a monotonic and consistent correlation between residues and fuel ethanol content is shown for different engine operating points (speed and load) and E0, E55 and E85 fuel blends. In particular, at the engine speeds of 1500RPM and 2500RPM, the generated residues has an approximate affine relationship with the ethanol content for the three fuel blends tested. At the engine speed of 2000RPM, a small nonlinearity can be observed for high-ethanol blends (E85).

The computed residues are able to isolate the charge cooling effect due to fuel vaporization while significantly reducing the influences of measurement and quantization noise, pressure sensor nonlinearities, pegging error, and unmodeled dynamics. Besides, the use of the residues allow a reduction in the model complexity and required calibration efforts. Consequently, the model will be mainly validated and calibrated in section V by comparing the residues generated from simulated and measured compression pressure data.

V. Experimental Results and Model Validation

In order to validate the model developed in Section III and determine the relationship between ethanol content and residues, experimental data were collected on a 2.0L Turbocharged SIDI VVT engine equipped Kistler 6125B in-cylinder pressure sensors. Dynamometer tests were conducted at different engine operating points (speed and load) under Single and Split injection modes for various gasoline-ethanol fuel blends.

The operating points selected to validate the model correspond to common engine operating conditions on typical driving cycles and are specified in terms of engine speed and intake mass airflow rate set-points: (1500RPM, 80kg/hr), (2000RPM, 100kg/hr), (2000RPM, 150kg/hr), (2500RPM, 130kg/hr) and (2500RPM, 170kg/hr). Table III summarizes the nominal test conditions. The end of 2nd injection in split mode, $\theta_{eoj[c_s]}$, was fixed at 140 CAdeg bTDC to ensure the intake valve is closed during injection while allowing the sufficient charge mixing necessary for a good combustion. The split factor between the two injections in split mode, SF_{inj}, set to be 50% responds to a tradeoff among combustion quality, minimum injection timing and detection sensitivity; however, no systematic optimization has been conducted for it.

TABLE III
Nominal Test Conditions

Variable	Description	Value
θ_{ivc}	Intake valve open	30 CAdeg bITDC[1]
θ_{evo}	Exhaust valve closure	20 CAdeg aITDC
P_{inj}	Fuel rail pressure	6 MPa
λ	AFR/AFR$_{\text{stoichiometric}}$	1
SF_{inj}	Injection split factor (Sp mode)	50%
$\theta_{soj[i_s]}$	Start of injection during intake	285 CAdeg bCTDC[2]
$\theta_{eoj[c_s]}$	End of 2nd injection (Sp mode)	140 CAdeg bCTDC
θ_{ign}	Ignition timing	MBT map for E0

[1] Intake Top Dead Center; [2] Combustion Top Dead Center

The results presented in this section were obtained from cylinder 4 measurements using a low-pass filter with normalized cutoff frequency of 0.1 and an averaging of 10 cycles. In this way, 7-10 residues could be computed for each condition and fuel blend given the available measurement duration. The averages of the residues for each operating condition and each blend were also computed. Note that, there are two levels of averaging: cycle and residue. The combination of both determines the detection time and accuracy. Further study needs to be performed to establish the optimal averaging arrangement. The measurements were also used to feed the model, simulate the compression stroke pressure traces and generate the simulated residues which were compared with the measured ones to calibrate and validate the model. The experimental measurements used as inputs for the model are: fuel rail temperature, $T_{fl,inj}$; intake air temperature, T_a; intake mass air flow, MAF; cylinder pressure at IVC, $P_{cyl,0}$; injected fuel mass, $m_{fl,inj}$; injection pulse, Sig_{Inj}; ignition pulse, Sig_{Ign}; engine speed, N_{eng}; and measured ethanol concentration, e.

The model calibration was performed in order to mini-

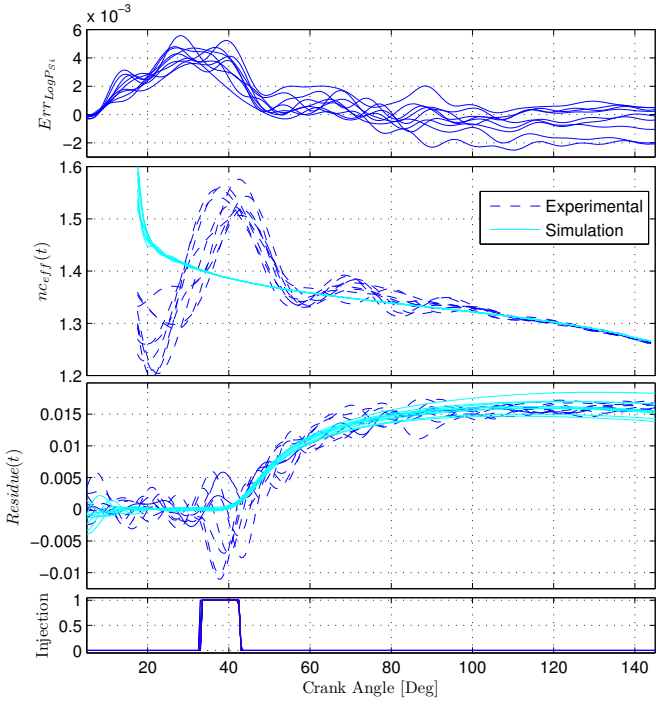

Fig. 4. Features used for the model Calibration. a) $Err_{LogP,Si}$ b) $n_{c,eff}$. c) $Residue(t)$. d) Injection pulse (not a tuning feature)

mize the error in the logarithm of the cylinder pressure in single injection mode, $Err_{LogP_{Si}}$, and to match the effective polytropic compression coefficient in single injection mode, $n_{c,eff}(t)$, and the time-varying residue, $Residue(t)$. Fig. 4 shows the features for the calibrated model for E0 (gasoline) at the (1500RPM, 80Kg/hr) engine operating point. The oscillations present in the experimental $n_{c,eff}(t)$ and $Residue(t)$ are caused by measurement noise, quantization, and engine disturbances, such as intake valve closure. In particular, cylinder pressure quantization has an important undesired effect on the $n_{c,eff}(t)$ calculation when the cylinder pressure varies slowly which results in the large oscillations that vanish toward the end of the compression stroke observed in Fig. 4.b.

The model calibration and results presented in this work were generated assuming a fixed value for the cylinder temperature at IVC for all fuel blends since the *IVC Cylinder Charge Model* has not yet been fully calibrated and integrated with the rest of the model. Table IV summarizes the tunable model parameters with their nominal values for three fuel blends, as well as the tuning constraints and most relevant feature used to calibrate each parameter.

TABLE IV
PARAMETER VALUES AFTER CALIBRATION

Parameter	Fuel Blend E0	E55	E85	Calibration constraints	Target feature
n_c	1.35	1.37	1.385	fixed[1]	Fig.4.a
β	⟵	16840	⟶	$\sim (N_{eng}, MAF)$	Fig.4.b
τ_d	0.3	0.5	0.7	$\sim (N_{eng}, MAF)$	Fig.4.c[2]
α	⟵	0.8	⟶	fixed[1]	Fig. 4.c[3]
k_{evap}	⟵	2.4	⟶	fixed[1]	Fig. 4.c[4]
$d_{\phi,0}$	100	105	135	$f(P_{inj}, P_{cyl})$	Fig. 4.c[4]

[1] Parameter value is fixed for all operating conditions; [2] Jump time
[3] Jump height and final shape; [4] Rise time and final shape

As the reader may foresee, the number of parameters and the complexity of the model can result in many different combinations of parameter values that optimize the tuning features. This ambiguity in the parameter calibration can be eliminated by imposing constraints to the parameter variation considering the underlying physical phenomena and by performing the calibration concurrently over a wide set of operating conditions. The constraints utilized are shown in Table IV, for instance, n_c is fixed for all the different operating conditions, while β can be adjusted proportionally to changes in speed and load. Note that, the initial droplet diameter, $d_{\phi,0}$, does not depend on the operating condition directly, but it is a function of the fuel rail pressure, P_{inj}, and cylinder pressure, P_{cyl}, during the injection period, instead. The determination of the functional form of $d_{\phi,0}$ was left for future work.

Fig. 5 presents experimental and simulated results for E0, E55 and E85 fuel blends at the (1500RPM,80kg/hr) engine operating point. Fig. 5.a shows the averaged mean-residue for each fuel blend together with the variability interval for individual mean-residue calculations; the lines are least squared linear regressions on the averaged values. Fig. 5.b illustrates the time-varying residues generated from simulated

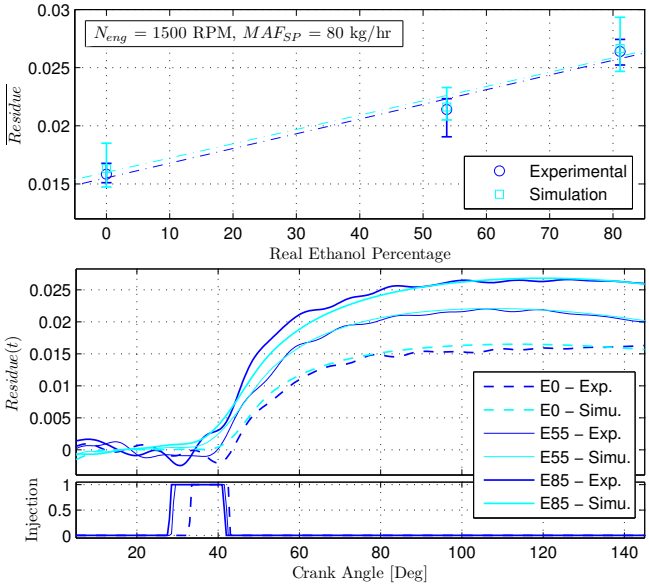

Fig. 5. Experimental and simulated results for 1500RPM-80kg/hr engine condition, and E0, E55 and E85 fuel blends. a) mean-residues b) Time-varying residues. c) Injection pulse

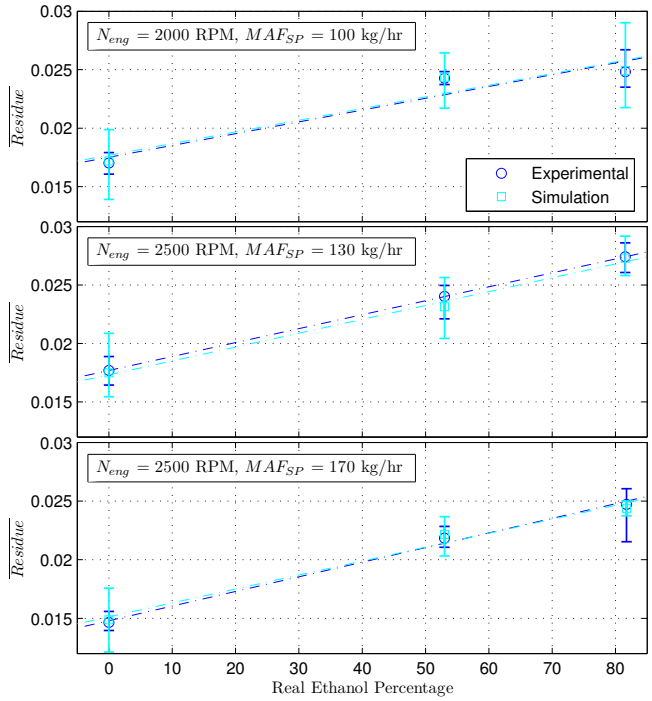

Fig. 6. Experimental and simulated mean-residues for three operating conditions, and E0, E55 and E85 fuel blends. a) 2000RPM-100kg/hr. b) 2500RPM-130kg/hr. c) 2000RPM-170kg/hr.

and measured cylinder pressure. Note that, while the mean-residue captures the overall effect and model behavior, it is the time-varying residue, $Residue(t)$, the one that allows to calibrate the model and evaluate its accuracy. The good match observed in the time-varying residue for the different fuel blends is a strong indication of the validity of the proposed model structure.

Fig. 6 shows mean-residue plots for additional engine operating points: (2000RPM, 100kg/hr), (2500RPM, 130kg/hr) and (2500RPM, 170kg/hr). A good match can be observed

between the experimental and simulated mean-residues for the three conditions, which demonstrates the model validity and its capability to capture the effect of ethanol concentration at different speeds and loads. Fig. 6.a also confirms the model is able to reproduce the nonlinear correlation between residue and ethanol content observed for E85 at the (2000RPM, 100kg/hr) operating point.

The variability observed in the experimental residues is caused by cycle-to-cycle variations in the combustion process. These variations affect the cylinder temperature and pressure after combustion, and eventually the exhaust gas temperature which after all influences the IVC cylinder charge conditions during the next cycle. As explained in the *IVC Cylinder Charge Model*, the evolution of the cylinder pressure and the fuel vaporization process both depend on the initial charge conditions at IVC, and thus, the residues are sensitivity to combustion fluctuations. However, the variability observed in the simulated residues is larger than in the measured ones. We attribute this difference to cylinder pressure pegging errors. The actual pegging procedure consists in matching the cylinder pressure at compression BDC with the instantaneous intake manifold pressure (MAP). This is a straight-forward and simple method, but many previous works have addressed its inaccuracy for IVC charge condition estimations [22][20][23]. The effect of this offset error in the pressure measurements is minimized in the residue computation as explained in Section IV. However, the inaccurate pegging introduces error in the simulation initial conditions which propagates through out the entire pressure evolution, and this propagation effect can not be canceled by the residue generation algorithm. Future work contemplates the use of a more precise pegging methodology [21] to mitigate this problem.

VI. Conclusions

A physics-based lumped-parameter model for the cylinder pressure evolution during the compression stroke in direct-injection (DI) engines was presented. The model captures the charge cooling effect due to fuel vaporization of ethanol-gasoline blends using a multi-component fuel model. A residue generation algorithm was also introduced to extract such charge cooling effect from cylinder pressure measurements during the compression stroke by exploiting two different injection patterns. Experimental data were collected for E0, E55 and E85 fuel blends on a 2.0L flex-fuel turbocharged SIDI VVT engine at various speeds and loads; and the residues calculated from measured and simulated cylinder pressure traces were compared.

The experimental residues show a monotonic and consistent correlation with the fuel ethanol content (e) for all the tested conditions. At 1500RPM and 2500RPM, the computed residues have an approximately affine relationship with the ethanol content, e, for the three fuels tested, while at 2000RPM a small nonlinear behavior can be observed for high-ethanol blends (E85). The comparison between experimental and simulated residues shows a good match for all the tested operating points and fuel blends, which proves the model capability to capture the effects of changes in ethanol concentration at different engine operating conditions.

Future work includes the extension of the proposed model to capture the effects of additional engine parameters, such as fuel rail pressure, and the implementation of a new cylinder pressure referencing method to address the problems of the current MAP-pegging approach and reduce the simulation variability. Furthermore, the possibility of using the model together with the residue generator to implement a model-based ethanol detection scheme will be investigated.

References

[1] J. S. Cowart, W. E. Boruta, J. D. Dalton, R. F. Dona, F. L. R. II, R. S. Furby, J. A. Piontkowski, R. E. Seiter, and R. M. Takai, "Powertrain development of the 1996 ford flexible fuel taurus," *SAE 952751*, 1995.

[2] A. C. Castro, C. H. Koster, and E. K. Franieck, "Flexible ethanol Otto engine, management system," *SAE 942400*, 1994.

[3] O. Volpato, F. Theunissen, and R. Mazara, "Engine management for flex fuel plus compressed natural gas vehicles," *SAE 2005-01-3777*, 2005.

[4] G. L. Seitz et al., "Method of determining the composition of fuel in a flexible fueled vehicle with an O2 sensor," *US Patent 5850824A*.

[5] W. D. Rotramel et al., "Method for determining the composition of fuel in a flexible fuel vehicle without an O2 sensor," *US Patent 5950599*.

[6] F. Theunissen, "Percent ethanol estimation on sensorless multi-fuel systems; advantages and limitations," *SAE 2003-01-3562*, 2003.

[7] K. ho Ahn, A. G. Stefanopoulou, and M. Jankovic, "Estimation of ethanol content in flex-fuel vehicles using an exhaust gas oxygen sensor: Model, tuning and sensitivity," in *Proceedings of Dynamic Systems and Control Conference (DSCC08)*, ser. Paper TuAT5.3, 2008.

[8] S. Washino et al., "Fuel properties detecting apparatus for an internal combustion engine," *US Patent 4905649*.

[9] H. Mitsumoto et al., "System and method for controlling ignition timing for internal combustion engine in which alcohol is mixed with gasoline," *US Patent 5050555*.

[10] L. Bromberg, D. Cohn, and J. Heywood, "Optimized fuel management system for direct injection ethanol enhancement of gasoline engines," *US Patent No. 7,225,787 B2*, June 5 2007.

[11] N. Oliverio, L. Jiang, H. Yilmaz, and A. Stefanopoulou, "Ethanol detection in flex-fuel direct injection engines using in-cylinder pressure measurements," *SAE 2009-01-0657*, 2009.

[12] J. Batteh and E. Curtis, "Modeling transient fuel effect with alternative fuels," *SAE 2005-01-1127*, 2005.

[13] R. Sontag, C. Borgnakke, and G. V. Wylen, *Fundamentals of thermodynamics*, 6th ed. John Wiley & Sons, Inc, 2003.

[14] J. B. Heywood, *Internal Combustion engines fundamentals*, 2nd ed. McGraw Hill, 1988.

[15] S. Tonini, M. Gavaises, C. Arcoumanis, A. Theodorakakos, and S. Kometani, "Multi-component fuel vaporization modelling and its effect on spray development in gasoline direct injection engines," *Proc. IMechE*, vol. 221, pp. 1321–1342, 2007.

[16] D. B. Spalding, *Combustion and Mass Transfer*, 1st ed. Pergamon Press, 1979.

[17] M. Locatelli, C. H. Onder, and H. P. Geering, "An easily tunable wall-wetting model for pfi engines," *SAE 2004-01-1461*, 2004.

[18] J. Senda, T. Higaki, Y. Sagane, H. Fujimoto, Y. Takagi, and M. Adachi, "Modeling and measurement on evaporation process of multicomponent fuels," *SAE 2000-01-0280*, 2004.

[19] J. Barata, "Modeling of biofuel droplets dispersion and evaporation," *Renewable Energy*, vol. 33, pp. 769–779, 2008.

[20] P. Oberg and L. Erikssons, "Control oriented modeling of the gas exchange process on variable cam timing engines," *SAE 2006-01-0660*, 2006.

[21] K. Lee, M. Kwon, M. Sunwoo, and M. Yoon, "An in-cylinder pressure referencing method based on a variable polytropic coefficient," *SAE 2007-01-3535*, 2007.

[22] J. F. Sinnamon and M. C. Sellnau, "A new technique for residual gas estimation and modeling in engines," *SAE 2008-01-0093*, 2008.

[23] M. J. Roelle, N. Ravi, and J. C. Gerdes, "Estimation thermodynamic state and ignition in HCCI with variable fuel injection timing," in *Proceedings of 2007 ASME International Mechanical Engineering Congress and Exposition*, Seattle, Washington, USA, 2007.